Cyclic shearing response of granular material in the semi-fluidized regime

Andres R. Barrero[1], William Oquendo[2], Mahdi Taiebat[3], and Arcesio Lizcano[4]

[1]Department of Civil Engineering, University of British Columbia, Vancouver, BC, Canada, email: abarrero@civil.ubc.ca
[2]Faculty of Engineering, Universidad de la Sabana, Bogotá, D.C., Colombia, email: william.oquendo@unisabana.edu.co
[3]Department of Civil Engineering, University of British Columbia, Vancouver, BC, Canada, email: mtaiebat@civil.ubc.ca
[4]SRK Consulting, Vancouver, BC, Canada, email: alizcano@srk.com

ABSTRACT

Liquefaction is a phenomenon usually observed in saturated granular soils when subjected to monotonic or cyclic shearing under constrained volumetric conditions. Liquefaction is usually associated with a loss of mean effective stress due to generation of excess pore pressure during the shearing of soil. In this process the particles reduce, or in the extreme case may lose, contact with each other. This nearly contact-free state is known as "semi-fluidized regime". In this state, the soil behaves almost like a viscous fluid, but the properties and origins of this response are not well understood. This study presents a series of numerical simulations using Discrete Element Method (DEM) to model the constant volume cyclic shearing of three granular assemblies with different packing fractions. The variations of the stress-strain response and the corresponding coordination number for each sample are tracked when the semi-fluidized regime is achieved. The results show the semi-fluidized regime in all of these assemblies regardless their packing fraction. This micro-mechanics based approach to the analysis can elaborate on the variations of the coordination number, mean effective stress, and developed shear strains before and after entering such regime.

INTRODUCTION

Understanding the fundamental mechanism of soil liquefaction is one of the major challenges among the geotechnical community. In general, liquefaction occurs on saturated granular soils when subjected to monotonic or cyclic loads, leading to a temporary or permanent loss of shear stiffness and strength in the soil matrix. Usually the temporary loss of strength is due to excessive generation of pore pressure. Soil liquefaction often leads to significant displacements, and this is one of the reasons of the considerable damage frequently seen after earthquake events. The current practice distinguishes 2 types of liquefaction: 1) flow liquefaction, and, 2) cyclic mobility (or cyclic liquefaction). The current study is focused on the mechanics behind the cyclic mobility. This type of liquefaction can be associated to almost any type of granular material,

even dense sands. It is characterized by its progressive reduction in the effective stress and progressive accumulation of shear deformation. A distinct feature of this type of liquefaction is the temporary loss of strength when the peak pore pressure rises momentarily in each cycle to the confining pressure, where the material generates significant shear strains. Although such state is commonly known as the "semi-suspend" state (Wang and Wei 2016), in this study will be refer to it as the semi-fluidized regime. To understand the underlying mechanism of the semi-fluidized regime, researchers have performed DEM simulations using particle disks (like Wang et al. 2016). However, their results were limited to 2-D simulations. In contrast, this study evaluates the semi-fluidized regime using 3-D DEM simulations, comparing qualitatively the numerical tool with the experimental results when applied to the semi-fluidized regime. The numerical tool used in this study is an open-source molecular dynamics code developed by Oquendo (2013). The code has been used to study the influence of rotations on the critical state of soil mechanics (Oquendo et al. 2011) and to derive an equation of state relating the compactivity to the packing fraction (Oquendo et al. 2016). The paper is structured as follows: in the first section, the numerical method and its fundamental contact laws underlying the DEM simulations are presented. Then, in the second section, the sample preparation and the shearing procedure are described. The third section present the main results, such as the deviatoric stress, mean stress and deviatoric strain and their relationship with the average particle contact which is used to characterize the semi-fluidized regime.

NUMERICAL METHOD

The Discrete Element Method (DEM) model the constituent particles of a granular material as distinct bodies with specific geometries which interact by (classical) laws. In the present study, the granular material is modelled as composed by three-dimensional (3D) spheres, with different radii (polydisperse), interacting via soft-particle laws. In this approach, a key quantity is the "interpenetration" of overlap of the particles, from which all the normal and tangential forces are derived. Given two particles, i and j of radii R_i and R_j, their overlap h_{ij} can be computed as

$$h_{ij} = R_i + R_j - \left|\vec{r}_{ij}\right| \tag{1}$$

where $\vec{r}_{ij} = \vec{r}_i - \vec{r}_j$, with $\vec{r}_i$ and $\vec{r}_j$ being the vector positions of the center of each particle. The displacements of the element boundary and the associated stresses are consequences of the motions of the particles. In this study, each particle i undergoes translational and rotational motions given by the absolute linear and angular velocities $\vec{v}_i$ and $\vec{\omega}_i$, respectively. The translational (rotational) motion of each particle is caused by the resultant force (torque) acting on the particle from its contacts with neighboring particles. The force acting at a contact (i, j) can be broken down into its components in the normal and tangential directions, $\vec{F}_{\text{norm}}$ and $\vec{F}_{\text{tan}}$, respectively. The normal component is along the unit vector $\hat{n}_{ij}$ joining the centers of the particles i and j,

$$\hat{n}_{ij} = \vec{r}_{ij}/|\vec{r}_{ij}| \tag{2}$$

and the tangential component $\hat{t}_{ij}$ perpendicular to $\hat{n}_{ij}$. Each one of the inter-granular normal and tangential forces consists of an elastic and a viscous part. The normal elastic force $\vec{F}_{\text{norm}}^{\text{elas}}$, representing the particle repulsive force, can be modelled linear, non-linear, hysteric, etc. For this work the simple linear form is used,

$$\vec{F}_{\text{norm}}^{\text{elas}} = k_n h_{ij} \hat{n}_{ij} \tag{3}$$

where k_n is the particle normal stiffness. The normal dissipative force $\vec{F}_{\text{norm}}^{\text{diss}}$, representing the dissipative term, is calculated from the normal component of the relative velocity $\vec{v}_{ij,n}$ and the normal damping coefficient γ_n by

$$\vec{F}_{\text{norm}}^{\text{diss}} = -\gamma_n \vec{v}_{ij,n} \tag{4}$$

For the tangential force model, some authors have used only the elastic component (Tokoro et al. 2005), while others have also included the dissipative component (Pöschel and Buchholtz 1993). In the present study, the tangential force is assumed to include both elastic and dissipative parts, analogous to the normal force configuration. The tangential elastic force $\vec{F}_{\text{norm}}^{\text{elas}}$, acting in the opposite direction of the inter-granular relative velocity $\vec{v}_{ij,t}$, is proportional to the tangential relative displacement δ_{ij} (partial slip), according to

$$\vec{F}_{\text{tan}}^{\text{elas}} = -k_t \delta_{ij} \hat{t}_{ij} \tag{5}$$

where

$$\delta_{ij} = \left|\int \vec{v}_{ij,t} dt\right|. \tag{6}$$

The tangential dissipative force $\vec{F}_{\text{tan}}^{\text{diss}}$, representing the dissipative term is modeled as followed

$$\vec{F}_{\text{tan}}^{\text{diss}} = -\gamma_t \vec{v}_{ij,t} \tag{7}$$

where γ_t is the tangential damping coefficient. In this study, we consider the normal stiffness to be equal to the tangential stiffness, an assumption that is used in a number of other DEM based studies of granular material (see e.g., Kwok and Bolton 2010 and Minh and Cheng 2014). The magnitudes of the normal and tangential forces at the particle contact are given by $\left|\vec{F}_{\text{norm}}\right| = \left|\vec{F}_{\text{norm}}^{\text{elas}} + \vec{F}_{\text{norm}}^{\text{diss}}\right|$ and $\left|\vec{F}_{\text{tan}}\right| = \left|\vec{F}_{\text{tan}}^{\text{elas}} + \vec{F}_{\text{tan}}^{\text{diss}}\right|$, respectively. If a Coulomb friction law is used at the

particle contacts and if μ_s is the particle-to-particle coefficient of sliding friction, the particles are in no-sliding condition when $|\vec{F}_{\text{tan}}| < \mu_s|\vec{F}_{\text{norm}}|$; they slide against each other when $|\vec{F}_{\text{tan}}| = \mu_s|\vec{F}_{\text{norm}}|$. This results in a linear spring-dashpot model with a sliding/static condition for the tangential forces.

The rotation of each particle is caused by the action of the torque that results from its contacts with neighboring particles. The torque acting on particle i at a contact (i, j) is the summation of the torque due to the tangential forces, $\vec{T}_{\text{tan}}$, the rolling resistance torque, $\vec{T}_{\text{roll}}$, and the dissipative torque of the angular velocity in the normal direction $\vec{T}_{\text{tor}}$. The equations used for torque are defined according to Luding (2008).

The total force and the total torque acting on particle i are given by

$$\vec{F}_i = \sum_{c\in i}(\vec{F}_{\text{norm}} + \vec{F}_{\text{tan}}) \quad (8)$$

$$\vec{T}_i = \sum_{c\in i}(\vec{T}_{\text{tan}} + \vec{T}_{\text{roll}} + \vec{T}_{\text{tor}}) \quad (9)$$

where c is the number of contacts of the particle. The dynamics of the particle i at any time t are governed by Newton's second law of motion as

$$m_i \frac{d\vec{v}_i}{dt} = \vec{F}_i \quad (10)$$

$$I_i \frac{d\vec{\omega}_i}{dt} = \vec{T}_i \quad (11)$$

where I_i is the moment of inertia of the particle and m_i is the particle mass.

SAMPLE CONSTRUCTION AND SHEARING

The purpose of the sample construction is to build isotropic granular assemblies subjected to the same confinement pressure with different degrees of compaction. The compactness is represented by the solid fraction Φ defined as

$$\Phi = \mathrm{V_g}/\mathrm{V} \quad (12)$$

where $\mathrm{V_g}$ is the volume occupied by the solid grains and V is the total volume. The solid fraction can be related to the void ratio with the expression, $e = (1/\Phi) - 1$. The sample construction and shearing consisted in three phases: a sample generation in which the grains are generated, followed by a densification phase to bring the sample to the desired compaction degree, finally the sample is cyclically sheared using a true-triaxial configuration. It is important to highlight that different sets of contact properties are used for the sample generation and in the true-triaxial cyclic shearing. In particular, the friction coefficient allows to control the final density of the sample (the lower the friction the denser the system). Table 1 shows the contact properties used

during the sample densification. In all simulations presented in this paper the gravity is set to zero. Furthermore, the particle-wall friction is also set to zero to avoid principal stress rotations.

Table 1. Contact parameters during the densification procedure

Parameter	Value
Density, ρ (kg/m^3)	2650
Normal stiffness, k_n (N/m)	1.0E5
Particle friction coefficient, μ_s	0.1,0.2,0.3
Particle rolling coefficient, μ_r	0.1
Restitution coefficient, ϵ	0.15

Sample generation

The samples are made of 4096 spheres with diameters uniformly distributed between 1mm and 2mm. Each grain is randomly placed in the nodes of a square grid of $16 \times 16 \times 16$ elements. The length of the grid elements is set to $1.12d_{\max}$, guaranteeing no overlap between the spheres during the sample generation.

Densification

During this phase, the walls were moved slowly with a constant velocity towards the center of the box. Additionally, each grain is assigned a randomly oriented initial velocity with the speed varying between 0 and 0.1 m/s. Once the compaction degree reaches $\Phi = 0.5$, the velocity-control condition of the walls is switch to a stress-controlled condition, where the walls were prescribed to $\sigma_{p0} = 100$ kPa. In order to have different compaction degrees, different values of friction coefficient μ_s are used, as shown in Table 1. The highest μ_s leads to the lowest solid fraction and the lowest μ_s leads to the highest solid fraction. A snapshot of the particle arrangements and the boundary condition at the end of the densification phase for the one of the final packing fraction is shown in Figure 1a.

True-triaxial cyclic shearing

After the construction of the sample was finalized, the particle friction coefficient μ_s is set to 0.5 for all three samples. All other contact parameters are kept as those presented in Table 1. These parameters are typically used to represent the mechanical behavior of sand (Wang and Gutierrez 2009, Sakakibara et al. 2009). Figure 1b shows the boundary conditions of the undrained true-triaxial test. During this test, the walls were slowly moved with a constant quasi-static velocity. Water was not simulated in this work, instead the total volume of the box was kept constant by keeping the velocity of the side walls as -0.5 times of that of the top wall. Consequently, if the top wall moves with $\vec{v}_z$, then the velocities of the side walls are:

$$\vec{v}_x = 0.5(-x/z)\vec{v}_z \quad (13)$$
$$\vec{v}_y = 0.5(-y/z)\vec{v}_z \quad (14)$$

controlling the walls velocity allows to keep the total volume constant throughout the test. The top wall velocity is set to remain in the quasi-static regime. To this end, the inertia parameter I is used according to:

$$I = \dot{\varepsilon}_z\sqrt{m/d\sigma_{p0}} \quad (15)$$

where $\dot{\varepsilon}_z = \vec{v}_z/z$ and d is the average particle size. The quasi-static limit is characterized by the condition $I \ll 1$ (MiDi 2004). In this study, for all simulations I remains below 10^{-3} during shear.

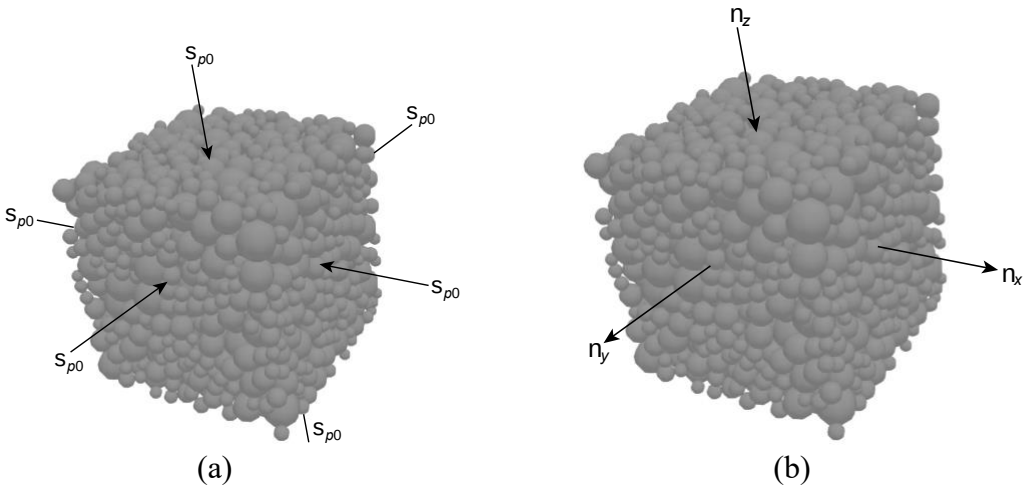

(a) (b)

Figure 1. Boundary conditions for (a) isotropic compression and (b) undrained shearing.

RESULTS

To link the micro-mechanical normal and tangential forces from the particle interactions to the macro-mechanical reponse of the granular material, the average stress tensor σ_{kl} of a selected volume V of the 3D element is calculated as follows

$$\sigma_{kl} = \frac{1}{V}\sum_{i\in N}\sum_{c\in i} F_k r_l^c \quad (16)$$

where the subscripts k and $l(= x, y, z)$ represent the components in an orthonormal reference frame; the r_l^c represents a branch vector from the particle center of mass to a contact point; the summation is performed over the contacts c, which cover all i contacts of each particle, and for all N particles inside the selected area V of the particle assembly. The true-triaxial mean and deviatoric stresses, p and q, are calculated from the principal stresses σ_{zz} and σ_{xx} (Eq.16) according to $p = (\sigma_{xx} + \sigma_{yy} + \sigma_{zz})/3$ and $q = (\sigma_{zz} - \sigma_{xx})$. The principal strains ε_{xx}, ε_{yy} and

ε_{zz} are calculated from the boundaries of the sample box as $\varepsilon_{xx} = \Delta x/x$, $\varepsilon_{yy} = \Delta y/y$, and $\varepsilon_{zz} = \Delta z/z$, and the deviatoric strain is calculated as $\varepsilon_q = (\varepsilon_{zz} - \varepsilon_{xx})$. Liquefaction is considered when the level of stress reach $p = 0.1$ kPa.

The results for the undrained cyclic shearing for different packing fractions are shown in Figure 2, with three columns (left-center-right) of subfigures, each one representing a packing fraction. The left, center and right columns correspond to the highest, medium and lowest packing fraction, respectively. The results are presented in terms of variations of mean stress p, deviatoric stress q, coordination number z_c, deviatoric strain ε_q, and the number of cycles. The coordination number represents the average number of contact per particle as:

$$z_c = \frac{1}{N}\sum_{i=1}^{N} N_i^c \tag{17}$$

where N_i^c is the number of contacts of the particle i, and allows to detect the loss of contacts inside the sample. The possibility to examine the variations of the coordination number during the course of loading is one of the beauties of discrete element modeling of such systems.

The results show a qualitative agreement of the micro-mechanical model to reproduce the initial state-dependent undrained cyclic shear response of granular samples in a macro-mechanical level. In particular, the number of cycles to reach liquefaction for the highest, medium and lowest packing fractions are 70, 3.5 and 1, respectively. Additionally, the micro-mechanical model appears to capture the expected macro-mechanical "butterfly" shape stress-path near the origin (see Figures 2a-2c). The result clearly show that at small levels of mean stress the coordination number z_c is reduced to its minimum. In other words, the numerical simulations reproduce the main phenomenon associate with liquefaction. This is a credit to the capability of the micro-mechanical model to reproduce what is known as cyclic mobility liquefaction in saturated granular materials.

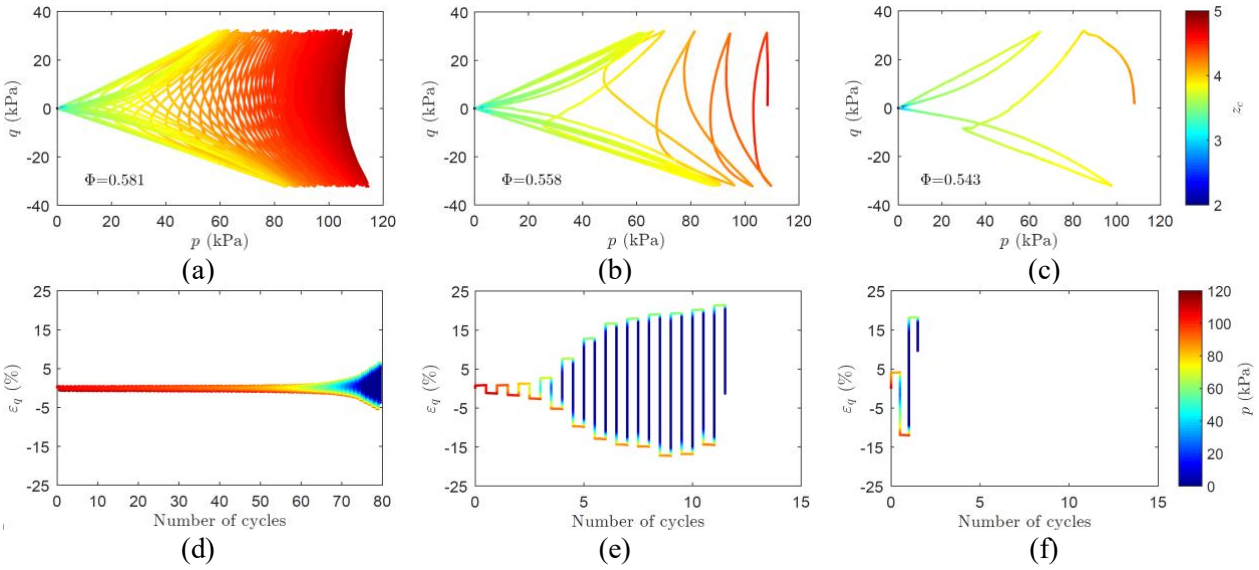

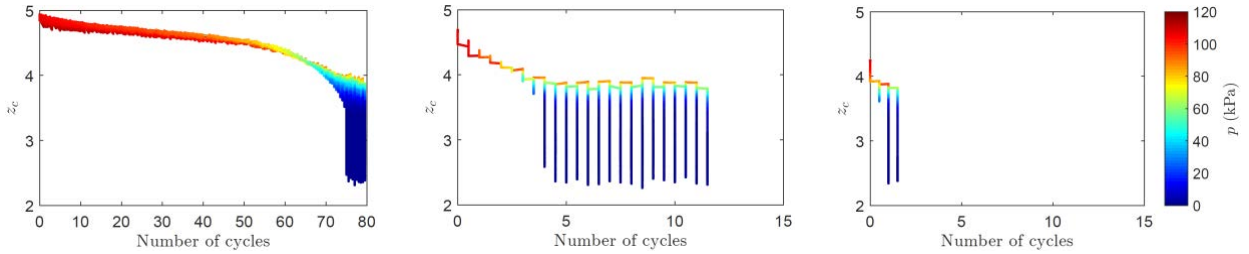

(g) (h) (i)

Figure 2. Results of cyclic shearing under constant volume for different packing fractions: (a-c) stress-path with color variation on coordination number, (d-f) deviatoric strain vs number of cycles with color variation on coordination number, and (g-i) evolution of coordination number with number of cycles with color variation on mean stress.

To explore in more detail the post-liquefaction response, the samples with highest and medium packing fractions were sheared for nine cycles beyond the designated liquefaction state in these analyses. Variations of the deviatoric strain ε_q and the number of cycles with the mean stress p are plotted in Figures 2d-2f for the highest, medium and lowest packing fraction, respectively. These figures show that the level of the mobilized deviatoric strain ε_q depends on the sample packing fraction. More specifically, the shear strain mobilized in the first post-liquefaction cycle for $\Phi = 0.543$ is beyond 10%, while for $\Phi = 0.581$ it is below 1%. Figures 2g-2i, show that the reduction of the coordination number also depends on the packing fraction. The lowest coordination number z_c is around 2.28 for all packings and it coincides with lowest mean stress. Furthermore, the results suggest that in the post-liquefaction cycles the influence of the packing fraction Φ on coordination number z_c vanishes.

The semi-fluidized regime can be understood as the region in which the mean stress very small. In such region, the momentarily loss of stiffness and strength leads to high generation of shear strains. The present micro-mechanical model appears to be capable of qualitatively presenting the mechanism of response associated with the semi-fluidized regime.

CONCLUSION

Three true-triaxial "numerical experiments" were conducted using molecular dynamics method for particle assemblies made up with polydisperse spheres with different packing fractions, to model the cyclic shearing under constant volume condition. The objective was to explore the state of the samples when they reach the "semi-fluidized" regime within the assembly of the particles where the resulting mean effective stress approaches very small values. To this end, simulation results were presented in terms of comparative variations of homogenized mean effective and shear stresses, shear strains, and coordination numbers with number of cycles for each sample. The results illustrate that the sample with higher packing fraction takes more cycles to reach the semi-fluidized regime. This sample also generates smaller amplitudes of shear strain. Most interesting is the variation of coordination number z_c within the assembly when reaching the semi-fluidized regime. At very small levels of mean effective stress the results show a

considerable drop of z_c below 4, that is the minimum expected for a balanced solid state, and this very well reflects the corresponding semi-fluidized nature of the assembly. Additional interpretation of the results is underway and it is expected to shed more light on the governing mechanism of response for the liquefaction phenomenon.

ACKNOWLEDGEMENT

Support to conduct this study is provided by the Natural Sciences & Engineering Research Council of Canada (NSERC) Canada and SRK Consulting.

REFERENCES

Kwok, C.-Y. and Bolton, M. (2010) *DEM simulations of thermally activated creep in soils.* Géotechnique, 60(6):425-433.

MiDi, G. D. R. (2004) *On dense granular flows.* European Physical Journal E-Soft Matter, 14(4).

Minh, N.H. and Cheng, Y.P. (2014) *A micromechanical study of the equivalent granular void ratio of soil mixtures using DEM.* InProceedings of the International Symposium on Geomechanics and Geotechnics: From Micro to Macro (pp. 219-224).

Ng, T.-T., Zhou, W., Ma, G., and Chang, X.-L. (2015). *Damping and particle mass in dem simulations under gravity*. Journal of Engineering Mechanics, 141(6):04014167.

Oquendo, W.F., Muñoz, J.D. and Lizcano, A. (2011) *Influence of rotations on the critical state of soil mechanics.* Computer Physics Communications, 182(9): 1860-1865.

Oquendo, W.F. (2013) *Micromechanical statistical study of the critical state in soil mechanics.* PhD thesis, Universidad Nacional de Colombia.

Oquendo, W., Munoz, J., and Radjai, F. (2016). *An equation of state for granular media at the limit state of isotropic compression*. EPL (Europhysics Letters), 114(1):14004.

Luding, S. (2007) *Cohesive, frictional powders: contact models for tension.* Granular Matter, 10(4), 235-246.

Pöschel, T. and Buchholtz, V. (1993) *Static friction phenomena in granular materials: Coulomb law versus particle geometry*. Physical Review Letters, 71:3963–3966.

Sakakibara, T., Shibuya, S., and Kato, S. (2009) *Effects of Grain Shape on Mechanical Behaviors of Granular Material under Plane Strain Condition in 3D DEM Analyses*. AIP Conference Proceedings, 1145(1):381–384.

Tokoro, C., Okaya, K. and Sadaki, J. (2005) *A fast algorithm for the discrete element method by contact force prediction*. Kona, 23:182–193.

Wang, J., and Gutierrez, M. (2009) *Modeling of scale effects on the micromechanics of granular media under direct shear condition*. AIP Conference Proceedings, 1145(1):365–368.

Wang, G., and Wei, J. (2016) *Microstructure evolution of granular soils in cyclic mobility and post-liquefaction process*. Granular Matter, 18(3):51.

Wang, R., Fu, P., Zhang, J.M. and Dafalias, Y.F. (2016) *Dem study of fabric features governing undrained post-liquefaction shear deformation of sand*. Acta Geotechnica, 11(6):1321–1337.